TÜBİTAK

Turkish Journal of Earth Sciences

http://journals.tubitak.gov.tr/earth/

Research Article

Turkish J Earth Sci
(2023) 32: 470-486

doi:10.55730/1300-0985.1856

Petrological characteristics of gabbroic intrusions in southeastern Urmia-Dokhtar magmatic belt, Kerman province, Iran: Evidence for post-Eocene mafic magmatism

Zahra NAJAFI[1,*], Hamid AHMADIPOUR[1], Abbas MORADIAN[1], Fatemeh SARJOUGHIAN[2], Kazuo NAKASHIMA[3]

[1]Department of Geology, College of Sciences, Shahid Bahonar University, Kerman, Iran
[2]Department of Earth Science, Faculty of Sciences, University of Kurdistan, Sanandaj, Iran
[3]Department of Earth and Environmental Science, Yamagata University, Yamagata, Japan

Received: 14.07.2022 • **Accepted/Published Online:** 13.04.2023 • **Final Version:** 29.05.2023

Abstract: At the south of the Bardsir, Kerman province, Iran, the southeastern part of the Urmia-Dokhtar magmatic arc (UDMA), a large number of gabbroic intrusions are intruded into the Eocene lava flows and pyroclastic rocks with the form of small stocks and dykes. In this paper, geochemical variations, magmatic evolutions, and the origin of these intrusions are investigated. The studied intrusions are characterized by fine-grained margins resulting from rapid cooling and flow differentiation. They display porphyritic texture and include coarse-grained clinopyroxene with diopside compositions (Wo = 46.89, En = 40.78, Fs = 12.32), plagioclase with labradorite composition (An = 54.14), and olivine in an intergranular crystalline groundmass. Their whole-rock chemistry proves that the rocks belong to the calc-alkaline series. The abundances of trace elements and REE, depletion of Nb, Ta, Zr, Ti, and Hf, and enrichment of LILE relative to HFSE indicate that these rocks belong to a subduction zone setting. Geochemical characteristics (Sm/Yb and La/Sm ratios) show that the source rock of these intrusions was the lithospheric mantle with spinel lherzolite composition, which initially underwent partial melting (10% to 20%) events and then was metasomatized by fluids derived from the subducting Neo-Tethys lithosphere.

Keywords: Gabbroic intrusion, Urmia-Dokhtar belt, Kerman province, Bardsir, Post-Eocene magmatism

1. Introduction

The geochemical characteristics and rock types of post-Eocene magmatism is one of the important issues that can help determine the geological evolutions of the southeast Urmia-Dokhtar magmatic arc. In the southeastern part of the Urmia-Dokhtar belt, called the Dehaj-Sarduieh magmatic belt (DSMB) in Kerman province, different magmatic episodes occurred after the Eocene period. These magmatic episodes include Jebal-E-Barez granitoids, Raviz-Shan Abad gabbro intrusions, volcanic rocks related to Bidkhan and Masahim volcanoes, dacitic plugs of Amir Al-Mo'menin Mountain, and Shah Khairullah Mountain (Daieparizi et al., 2021).

One of these magmatic events is the intrusion of gabbroic bodies that are injected into the Eocene lava flows and related pyroclastic rocks, in the form of irregular or dyke-like intrusions. Based on field observations it is clear that these gabbroic magmas were injected after the formation of an extrusive sequence.

Gabbros can occur in various tectono-magmatic settings including 1) Ophiolite-related layered and isotropic gabbros located in active orogenic areas (McBirney, 2009). 2) Gabbros of Alaskan-type assemblages in subduction-zone areas (Deng et al., 2014). 3) Postcollision gabbros (Yang et al., 2014). 4) Gabbros of large stratiform assemblages in nonorogenic areas. 5) Within-plate gabbros such as Wadi Shianite area, southeastern Desert, Egypt (Basta, 2015). Each of these gabbroic complexes has different geochemical properties, and some authors have used these properties to identify the nature of their mantle source and their tectono-magmatic environments (Deng et al., 2014).

Throughout the Urmia-Dokhtar magmatic arc, (UDMA), there are numerous post-Eocene granitic to gabbroic intrusions and several studies have been conducted on them (Kananian et al., 2014; Babazadeh et al., 2017, 2021; Fazlnia, 2019; Raeisi et al., 2021; Fazli et al., 2022). The ages of these intrusions vary from the early Oligocene to the late Miocene, and the researchers attribute their formation to the supra-subduction zone environment and consider that they emplaced at presyn or postcollision tectonic setting.

* Correspondence: najafi.zg@sci.uk.ac.ir

In the Dehaj-Sarduieh magmatic belt (DSMB), the pulses of mafic intrusive magmatism also can reflect important processes in the mantle beneath the Iranian continental crust and show the processes that occurred in the upper mantle or in the lower crust before and after collision. Although a number of these events have been studied in other parts of the DSMB, such as Raviz-Shanabad and Rafsanjan (Salehi Nejad et al, 2021), so far many of these masses at the south of Bardsir (Sang-e-Sayad region) have not been studied in petrological characteristics and their tectonic setting. This study examines the field characteristics and petrography of these massifs, their chemical compositions and evolution related to the order of crystallization of minerals, the tectono-magmatic setting, and the evolution of their parent magmas. Clarifying these features for the magmatic events could shed light on the post-Eocene magmatic history of this area and provide a basis for further studies.

2. Geological setting

The study area is located at south of Bardsir of the Kerman province, which forms the central part of the Dehaj-Sarduieh magmatic belt (DSMB) (Dimitrijevic, 1973) or the Kerman Cenozoic magmatic arc (KCMA; Shafiei et al., 2008). The DSMB approximately 500 km long and about 80 km wide, is located on the southern margin of the Central Iranian microcontinent. This magmatic belt was formed due to the subduction of the Neo-Tethys oceanic crust beneath the Central Iranian plate (Berberian and King, 1981; Alavi, 1994).

The most extensive rock formations of this belt are a thick sequence of volcanic and sedimentary rocks belonging to the Lower-Middle Eocene, Middle-Upper Eocene, and Oligocene, which are called the Bahr-Aseman, Razak and Hezar complexes, respectively (Dimitrijevic, 1973). Extensive magmatic pulses, emplacement and injection of intrusive masses after the Eocene with various compositions of mafic (such as gabbroic intrusions studied in this work) to felsic, are special features of this magmatic belt, so it is important to this study.

These gabbroic intrusions are located in south of Bardsir and in the central part of the DSMB (Figure 1). The oldest units in this area, based on the study of microfossils, include Late Cretaceous flysch-type sedimentary rocks (Afsharianzadeh and Etemadi, 1992). Units of the Hezar complex cover other parts of the study area. These gabbroic bodies intruded the Hezar complex, forming the uppermost part of the Eocene formation; it consists of folded sequences of volcano-sedimentary rocks with more than 1500 m in thickness (Dimitrijevic, 1973). Active tectonics in the region have caused numerous folds and fractures, resulting in extensive erosion and alteration.

3. Analysis methods

After field studies, the samples were divided into different groups of lavas and intrusions. Among these groups, ten fresh gabbro samples were sent to the Zarazma Mahan laboratory for whole rock chemical analysis. Alkaline fusion method was used to prepare and measure the major oxides. In this method, the sample is fused using lithium metaborate and the product is measured using ICP-OES (735 Variant Australia) after dissolution with nitric acid, and then the amounts of the major oxides are determined. To obtain trace-element abundances, the multi-acid method and Microwave digestion were used and then the final solution was analyzed with Agilent 4500 ICP-MS.

Polished thin sections were prepared for electron microprobe analyses on the minerals of the studied gabbros. Mineral chemical compositions were determined using JEOL JXA-8900 electron probe micro-analyzer at Yamagata University. Operating conditions were an accelerating voltage of 15 kV, a specimen current of 15 nA, and a beam diameter of 3 mm. The following standards were used for X-ray analysis: apatite, SiO2, TiO2, Al2O3, Cr_2O_3, PbVGe-oxide, Fe_2O_3, MnO, MgO, NiO, wollastonite, Ba-glass, $SrTiO_3$, albite, adularia, CaF_2, and NaCl. Data were processed by on-line computer using Oxide ZAF in the XM-89 PAC program composed by JEOL. Under the conditions described, analytical errors are ±2% for major elements and ±5% for trace elements.

4. Results

4.1. Field characteristics and petrography of gabbroic intrusions

Extensive detailed field studies show that this magmatic assemblage comprises alternations of lava flows with basaltic to andesitic compositions, agglomerate, tuff, and ignimbrite with layers of monolithic limestones and epiclastic shales, and sandstones. This alternation indicates that volcanic activities were periodic, and after each eruption, the volcanic material has eroded and formed epiclastic sediments in the adjacent shallow environments. These volcano-sedimentary assemblages were injected by Oligocene age granitoid (Sepidbar et al., 2019) stocks and mafic to felsic dykes (Figure 2-a).

The faults of the region show three directions: northwest-southeast, north-south, and northeast-southwest. A rose diagram was prepared from 167 measured faults in the study area (Figure 2-b). As shown in this diagram, the predominant trend of fractures is northeast-southwest. These dominant fractures probably have an extensional component, and the studied gabbroic intrusions were injected in the direction of these fractures.

The studied gabbroic intrusions crosscut all lithologies of the area (sedimentary and volcanic rock units and the Oligocene age granitoids (Figures 1 and 3-a). In the

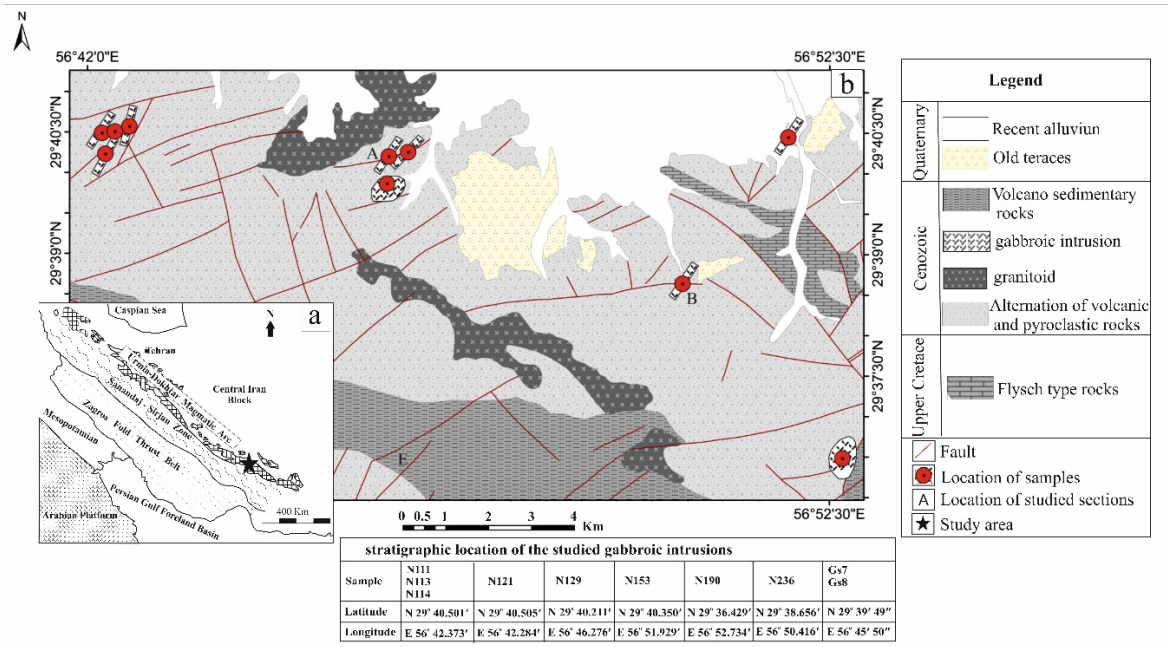

stratigraphic location of the studied gabbroic intrusions

Sample	N111 N113 N114	N121	N129	N153	N190	N236	Gs7 Gs8
Latitude	N 29° 40.501′	N 29° 40.505′	N 29° 40.211′	N 29° 40.350′	N 29° 36.429′	N 29° 38.656′	N 29° 39′ 49″
Longitude	E 56° 42.373′	E 56° 42.284′	E 56° 46.276′	E 56° 51.929′	E 56° 52.734′	E 56° 50.416′	E 56° 45′ 50″

Figure 1. (a) Location of the study area in the map of Iran (star). (b) Local geological map of the study area (adapted from the map of 1.100000 Bardsir, Afsharianzadeh and Etemadi, 1992).

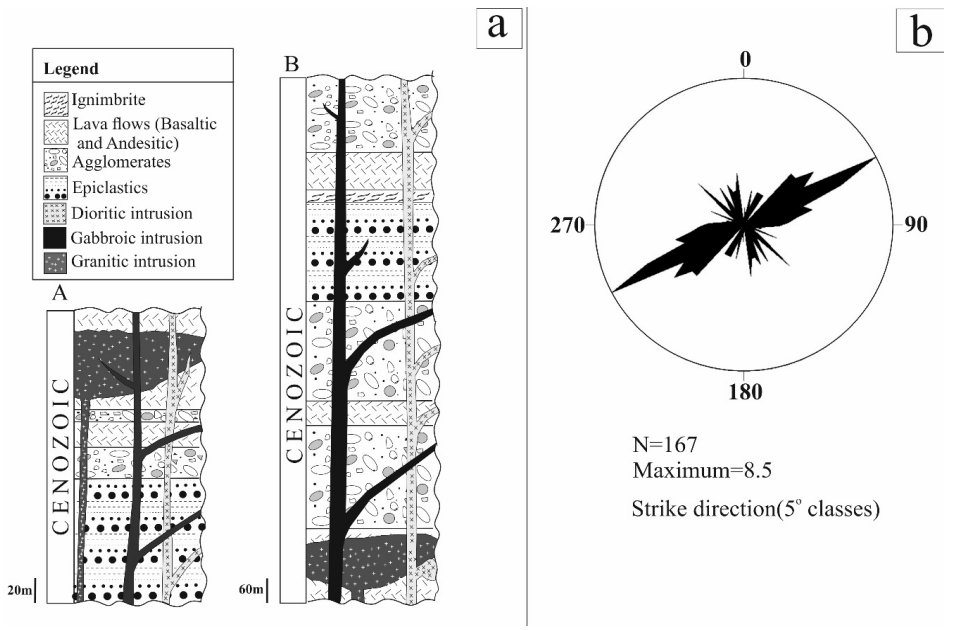

Figure 2 .(a) Studied columns in the two locations of the study area. (b) Rose diagram prepared from 167 measured faults in the study area, which shows the dominant northeast-southwest trend.

field, they occur as irregular masses and dykes, brown in altered/weathered and dark gray to black on fresh surfaces. The very fine-grained (microcrystalline) contact with the host rock indicates rapid quench at the margins (Figure 3-b). The diameter of the masses reaches up to 20 m, the thickness of the dykes is about 2 to 3 m and can be traced up to 80 m laterally. In the field, a considerable abundance of coarse-grained euhedral black pyroxene crystals (up

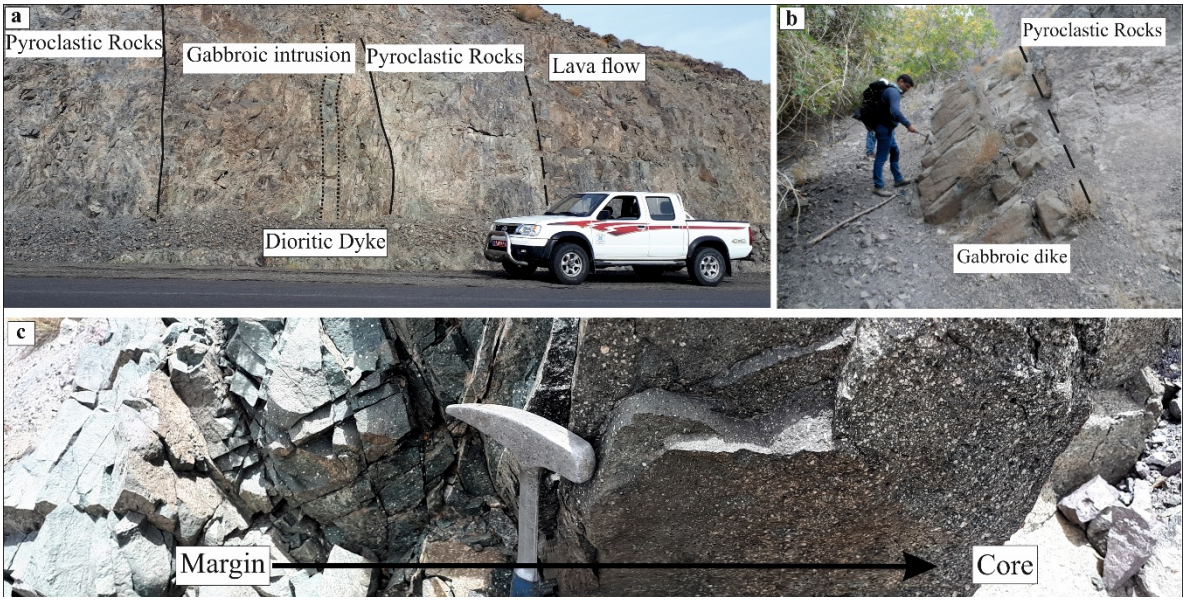

Figure 3. (a) Gabbroic intrusion that has penetrated into the pyroclastic rocks of the region. (b) Exposure of a gabbroic intrusion which intruded as a dyke in pyroclastic host rocks. (c) Flow differentiation and concentration of coarse-grained minerals in the center of the gabbroic dyke.

to 1 cm in size) are visible. In addition, they contain fine-grained subhedral plagioclases (less than 2 mm in size) and altered olivines in a fine-grained groundmass. The amount of pyroxene, plagioclase, and olivine in these rocks varies in each intrusion. In the gabbroic dykes, there is a clear flow differentiation, in which the size of the plagioclase is larger from the margins of the dyke toward its center, and the pyroxene crystals are concentrated mainly in the middle parts (Figure 3-c). The studied gabbros are dense with a dark gray to black appearance. In their specimens, the white-colored plagioclase and black-colored pyroxene crystals are set in a fine-grained dark gray matrix, and the olivine crystals are brown due to alteration.

Petrographic studies show that the studied intrusions are gabbros with distinct porphyritic textures in which plagioclase (45 vol%,), clinopyroxene (20 vol%), and olivine (5 vol%), as the main phases are located in a crystalline fine-grained groundmass. The groundmass is composed of small plagioclases and clinopyroxenes along with secondary and Fe-Ti oxides. In the groundmass, the small blades of plagioclase are arranged in such a way that they intersect each other and fill between them with anhedral clinopyroxene crystals and form an intergranular texture. Accessory minerals are magnetite, apatite, and zircon and secondary phases are epidote, calcite, and chlorite.

Euhedral to subhedral olivine crystals, with a size of 0.5 to 1 mm, (Figure 4-a) are mainly altered to bowlingite and iddingsite assemblages; only some have survived. All samples have euhedral to subhedral clinopyroxene with 1 to 5 mm in size, however, sometimes they altered to epidote and chlorite. Some of them show twining, zoning and resorbed in rims (Figure 4-b). The existence of plagioclase and olivine inclusions in clinopyroxene, form a poikilitic texture, which indicates that they probably crystallized before clinopyroxene oikocrysts (Figure 4-c).

Plagioclase crystals, appear as elongated euhedral to subhedral crystals with polysynthetic twinning in various sizes up to 8 mm. These crystals have unequilibrated textures, such as different forms of sieve texture, resorption and adsorption shapes, and compositional zoning. The presence of different shapes of plagioclases in a sample indicates that there are several generations of plagioclase in these rocks. The first shape (Plg1), shows compositional zoning, and its center shows dusty and corroded textures with clear rims)Figure 4-d(. The second shape (Plg2), is larger and has a coarse sieve texture (Figure 4-d) and the third shape (Plg3) appears as clear crystals, in equilibrium with the groundmass, showing no disequilibrium textures, such as sieve and absorption rims (Figure 4-d). The last shape probably crystallized simultaneously with small groundmass plagioclases and the clear margins of Plg1. Some plagioclase crystals have been altered and replaced by epidote and calcite. Some studied samples include coarse-grained orthopyroxene crystals. All orthopyroxenes are surrounded by an amphibole corona (Figure 4-e).

Semirounded olivine-clinopyroxene bearing enclaves are present in them. The diameter of the enclaves reaches up to 1 cm and contain interlocking crystals of altered olivine and clinopyroxene (Figure 4-f); they are mineralogically similar to host rocks and may be comagmatic enclaves

formed in the early stages of crystallization of the studied gabbros' parent magmas.

4.2. Mineral chemistry

Plagioclase and clinopyroxene were analyzed by electron microprobe and the results are given in Table 1. The composition of plagioclases has a relatively limited spectrum, and their An% values vary between 50 and 62, meaning they are labradorite.

The composition of clinopyroxenes of the studied gabbros is given in Table 2. The composition of these minerals is determined by the values of Fs = 11–14, En = 40–42, Wo = 44–48 and they are in the diopside-salite range. Al_2O_3 and TiO_2 vary from 2.64 to 4.78 wt.% and 0.74 to 0.95 wt.%, respectively. In general, the chemical composition of these clinopyroxenes is similar to that of calc-alkaline series rocks.

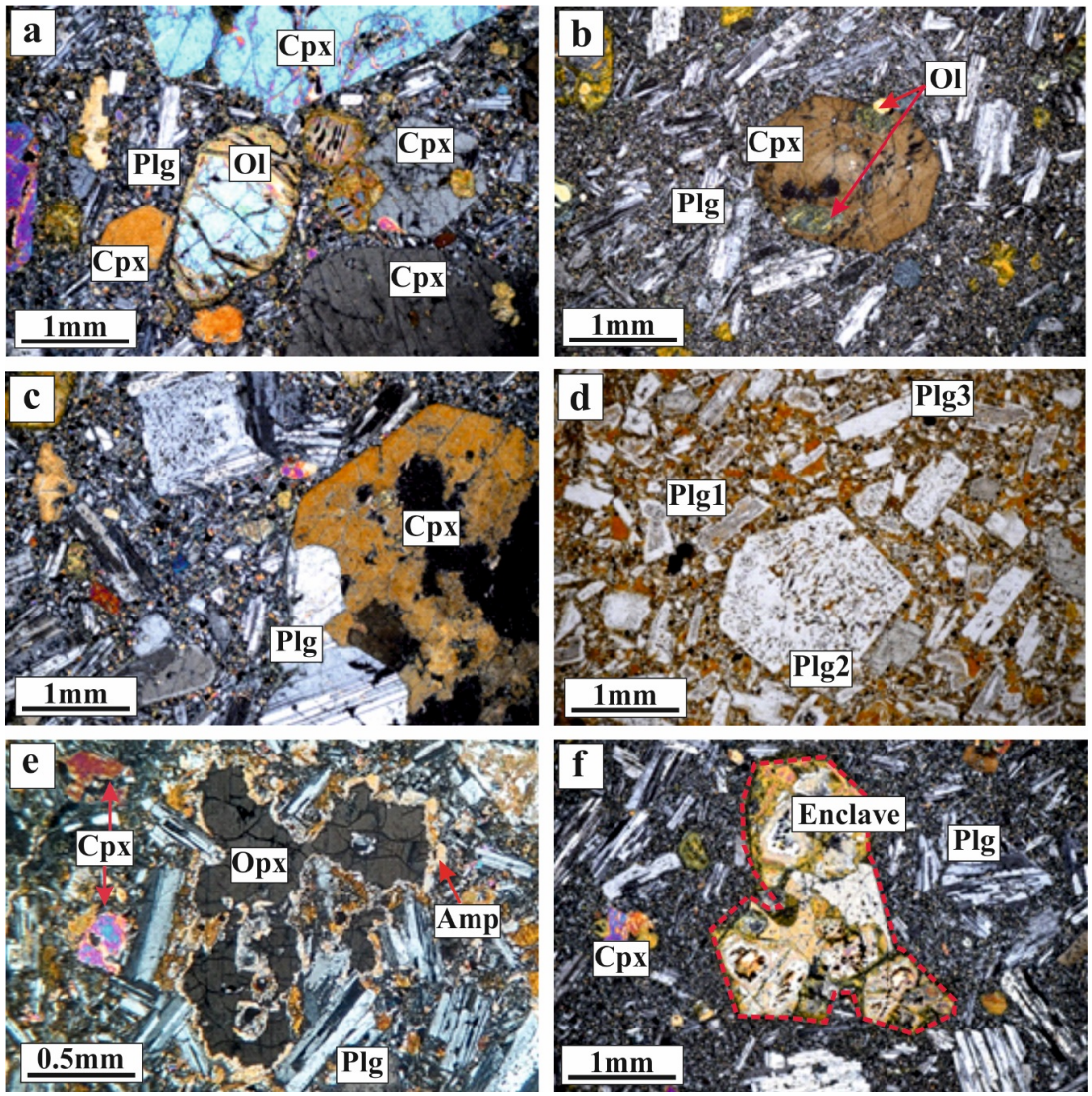

Figure 4. Transmitted light photomicrographs of (a) subhedral olivine crystals that have been altered to bowlingite and iddingsite in rim along with clinopyroxene crystals (crossed polarized light). (b) Clinopyroxene with zonation and inclusions of altered olivine (crossed polarized light). (c) Plagioclase and clinopyroxene crystals showing equilibrium texture (crossed polarized light). (d) Different shapes of plagioclases in the studied gabbro: Plg1 with dusty texture in the center and clear rim, Plg2: euhedral with coarse sieve texture, Plg3: without sieve texture (plane polarized light). (e) The orthopyroxene surrounded by the amphibole corona (Crossed polarized light). (f) Semrounded olivine-clinopyroxene bearing enclave (crossed polarized light). Abbreviation for names of minerals is derived from Whitney and Evans (2010).

Table 1. Composition of representative plagioclase from the Bardsir gabbroic intrusions by microprobe analysis (Structural Formula based on 8 Oxygen).

Plagioclase								
Rock	Gabbro							
Point	GS8-26	GS8-28	GS8-37	GS8-311	GS8-71	GS8-75	GS8-77	GS8-79
SiO_2	53.16	54.80	53.67	52.21	55.26	54.75	54.78	54.90
TiO_2	0.05	0.09	0.02	0.04	0.08	0.10	0.07	0.11
Al_2O_3	28.53	27.86	29.48	30.09	27.84	28.13	28.03	27.96
FeO	0.69	0.63	0.60	0.63	0.61	0.55	0.48	0.66
MnO	0.00	0.01	0.00	0.00	0.03	0.00	0.03	0.03
NiO	0.04	0.09	0.00	0.01	0.03	0.14	0.00	0.00
MgO	0.02	0.04	0.03	0.04	0.06	0.06	0.03	0.05
CaO	11.76	10.65	12.10	13.25	10.76	10.76	10.85	11.07
Na_2O	4.64	5.46	4.65	4.26	5.13	4.75	5.46	5.10
K_2O	0.31	0.40	0.44	0.30	1.11	0.92	0.64	0.46
Total	99.20	100.02	100.99	100.83	100.89	100.15	100.37	100.36
Si	2.43	2.48	2.42	2.36	2.49	2.48	2.48	2.48
Ti	0.00	0.00	0.00	0.00	0.00	0.00	0.00	0.00
Al	1.54	1.49	1.56	1.61	1.48	1.50	1.49	1.49
Fe^{2+}	0.03	0.02	0.02	0.02	0.02	0.02	0.02	0.03
Ca	0.58	0.52	0.58	0.64	0.52	0.52	0.53	0.54
Na	0.41	0.48	0.41	0.37	0.45	0.42	0.48	0.45
K	0.02	0.02	0.03	0.02	0.06	0.05	0.04	0.03
An	57.30	50.72	57.51	62.19	50.40	52.60	50.49	53.08
Ab	40.92	47.03	40.02	36.15	43.43	42.02	45.99	44.29
Or	1.78	2.24	2.47	1.65	6.17	5.37	3.52	2.63

4.3. Whole-rock geochemistry

Whole-rock major and trace element compositions are shown in Table 3. In the total alkali-silica (TAS) diagram (Cox, 1979) (Figure 5-a), all samples fall into the gabbro field. Most samples belong to the calc-alkaline series, and some of them are located in the potassium-rich calc-alkaline series field (Figure 5-b). To confirm the magmatic series of the samples, diagrams related to the chemical composition of clinopyroxenes were used. In these diagrams, the most studied samples fall into the subalkaline and calc-alkaline series (Figure 5-c, d). Also, the trace element ratios, such as La/Yb (>4.4) and Th/Yb (>0.7), display data related to calc-alkaline magmatic series (Ross and Bédard, 2009). The average values in the studied samples are 9.97 and 2.64, respectively. In general, the data of the major elements indicate that the studied rocks crystallized from evolved melts that have passed degrees of magmatic differentiation because of the moderate SiO_2 (avg: 48.17 wt%), high Al_2O_3 (avg:18.17 wt%), and low Mg # (avg: 33.26).

The chondrite-normalized patterns of REE in the studied samples are similar and all enriched in LREE relative to HREE (Figure 6-a), so that the ratios of $(La/Nd)_N$, $(La/Sm)_N$, and $(Gd/Yb)_N$ in them are equal to 2.50, 3.96, and 1.15, respectively, with no significant Eu anomaly. Furthermore, the studied rocks, like arc-related magmas, are enriched in some LILE (such as Ba) and depleted in HFSE, such as Nb, Ta, Zr, Ti, and Hf. These characteristics distinguish these rocks from MORB and OIB rocks (Figure 6-b). According to Figure 6, the chondrite-normalized patterns of HREE in the studied rocks are flat. In addition, LREE and LILE are clearly enriched relative to MORB, while HREE and HFSE, are depleted relative to MORBs. Instead, the normalized values of HREE and HFSE in these rocks are similar to those back-arc basalts, while the

Table 2. Composition of representative clinopyroxenes from the Bardsir gabbroic intrusions by microprobe analysis (Structural Formula based on 6 Oxygen).

Clinopyroxene										
Rock	Gabbro									
Point	GS8-21	GS8-23	GS8-25	GS8-32	GS8-34	GS8-36	GS8-61	GS8-63	GS8-65	GS8-67
SiO_2	51.63	50.86	51.83	51.31	51.05	51.50	51.05	50.99	48.25	50.54
TiO_2	0.76	0.93	0.85	0.74	0.88	0.86	0.77	0.84	0.91	0.95
Al_2O_3	2.67	3.79	2.64	3.33	3.30	2.95	3.05	3.57	4.78	3.39
FeO	10.10	9.77	9.10	9.06	9.87	9.37	10.43	9.97	10.85	9.39
MnO	0.31	0.24	0.22	0.27	0.13	0.29	0.36	0.16	0.34	0.13
NiO	0.00	0.00	0.00	0.05	0.00	0.09	0.01	0.00	0.06	0.00
MgO	13.19	12.91	13.27	13.40	13.09	13.79	12.85	12.86	13.25	13.20
CaO	21.25	20.72	21.81	21.31	21.03	21.39	20.66	20.87	19.23	21.53
Na_2O	0.53	0.49	0.37	0.39	0.45	0.45	0.51	0.45	0.37	0.36
K_2O	0.02	0.02	0.01	0.03	0.04	0.04	0.02	0.03	0.04	0.01
Total	100.46	99.72	100.10	99.89	99.85	100.72	99.71	99.73	98.08	99.50
Si	1.92	1.90	1.93	1.91	1.91	1.91	1.92	1.91	1.84	1.90
Ti	0.02	0.03	0.02	0.02	0.02	0.02	0.02	0.02	0.03	0.03
Al	0.12	0.17	0.12	0.15	0.15	0.13	0.14	0.16	0.21	0.15
Fe^{+3}	0.09	0.09	0.09	0.09	0.09	0.09	0.09	0.09	0.09	0.09
Fe^{+2}	0.23	0.22	0.20	0.20	0.22	0.20	0.24	0.23	0.26	0.21
Mn	0.01	0.01	0.01	0.01	0.00	0.01	0.01	0.00	0.01	0.00
Mg	0.73	0.72	0.74	0.75	0.73	0.76	0.72	0.72	0.75	0.74
Ca	0.85	0.83	0.87	0.85	0.84	0.85	0.83	0.84	0.78	0.87
Na	0.04	0.04	0.03	0.03	0.03	0.03	0.04	0.03	0.03	0.03
K	0.00	0.00	0.00	0.00	0.00	0.00	0.00	0.00	0.00	0.00
Wo	46.90	46.93	48.24	47.51	46.96	46.79	46.38	47.02	43.70	47.76
En	40.51	40.68	40.83	41.56	40.65	41.98	40.16	40.31	41.88	40.75
Fs	12.60	12.39	10.93	10.93	12.38	11.23	13.46	12.67	14.41	11.48
Al(IV)	0.06	0.07	0.04	0.06	0.07	0.07	0.06	0.07	0.14	0.08
Al(VI)	0.06	0.10	0.07	0.08	0.08	0.06	0.07	0.09	0.08	0.07
Mg#	56.65	56.91	59.30	59.67	57.00	59.54	55.20	56.34	54.99	58.44

amount of LREE and LILE in them is higher than these basalts.

5. Discussion

5.1. Magmatic evolution

Mineralogical, petrographic, and geochemical characteristics of gabbroic intrusion originated from common mafic magmas. Likely in chondrite-normalized REE diagrams, the patterns of REE abundances in these rocks are almost similar (Figure 6-a). These geochemical results prove that magmatic differentiation has played a role in the evolution of their parent magmas. The studied rocks originated from a common source and were created by the differentiation of magma. However, the Al_2O_3 and TiO_2 variations are

Table 3. Whole rock chemical analysis of the Bardsir gabbroic intrusions.

Sample	N111	N113	N114	N129	N190	GS7	GS8	N 121	N153	N236
wt%										
SiO_2	46.82	45.60	48.28	48.17	49.48	50.14	48.39	45.92	51.69	47.25
TiO_2	1.14	1.08	1.19	1.03	1.09	1.03	1.11	0.72	0.84	0.91
Al_2O_3	17.92	17.37	19.50	17.34	17.38	17.85	16.67	18.92	18.48	20.28
FeO	6.98	6.98	6.11	6.71	6.07	5.49	5.54	5.53	6.22	6.29
Fe_2O_3	3.03	2.95	2.62	3.12	3.21	3.14	2.86	2.45	3.44	2.52
BaO	0.07	0.07	0.07	0.04	0.04	0.08	0.08	0.03	0.03	0.02
CaO	10.13	11.06	9.33	8.55	9.46	8.39	9.36	10.02	8.90	11.59
K_2O	0.87	0.79	0.87	1.11	2.00	2.60	2.11	0.69	1.93	0.69
MgO	5.39	5.47	5.51	5.17	3.33	4.86	5.16	3.49	2.64	3.83
MnO	0.43	0.46	0.21	0.24	0.29	0.20	0.24	0.13	0.17	0.16
Na_2O	2.39	2.36	2.22	2.61	2.66	2.66	2.42	2.78	2.96	1.97
P_2O_5	0.48	0.61	0.30	0.38	0.60	0.32	0.32	0.17	0.16	0.24
SO_3	<0.05	0.10	<0.05	<0.05	0.07	0.06	0.08	<0.05	0.08	0.09
Cr_2O_3	0.01	0.01	0.01	<0.01	<0.01	<0.01	0.01	<0.01	<0.01	<0.01
LOI	3.42	4.17	2.93	4.62	3.50	2.44	4.91	8.47	1.71	3.41
Total	99.08	99.08	99.15	99.09	99.18	99.26	99.26	99.32	99.25	99.25
FeOt	9.74	9.67	8.50	9.55	8.99	8.35	8.14	7.75	9.34	8.59
ppm										
As	1.90	0.90	1.20	2.50	5.70	1.10	1.90	3.80	3.80	3.20
Ba	609	568	588	384	325	583	611	358	284	215
Be	1.40	1.40	1.40	1.00	1.50	1.50	1.40	0.60	0.60	0.50
Cd	0.80	0.80	0.80	0.80	0.80	0.70	0.90	0.10	0.10	0.10
Ce	69.0	67.0	67.0	430	78.0	72.0	78.0	37.0	29.0	33.0
Co	29.1	33.5	29.4	26.9	26.1	26.2	25.6	30.4	28.2	34.1
Cr	55.00	48.0	51.0	36.0	42.0	31.0	68.0	31.0	27.0	26.0
Cs	10.00	12.6	10.6	2.90	0.70	6.00	2.10	0.50	0.50	0.90
Cu	78.00	92.0	101	58.0	115	54.0	64.0	84.0	45.0	49.0
Dy	4.38	4.67	4.13	3.17	5.70	4.13	4.21	4.48	4.52	4.11
Er	2.65	3.04	2.66	2.00	3.84	2.48	2.74	2.40	2.93	2.23
Eu	1.21	1.33	1.24	0.92	1.40	1.25	1.16	1.19	1.14	1.26
Gd	3.83	4.33	3.44	3.12	5.08	4.25	4.06	3.95	3.95	3.66
Hf	2.54	2.55	2.34	1.48	4.16	3.20	2.95	2.99	3.12	1.61
La	36.0	36.0	34.0	22.0	36.0	37.0	39.0	16.0	12.0	15.0
Li	44.00	43.0	33.0	47.0	19.0	18.0	19.0	32.0	13.0	33.0
Lu	0.39	0.43	0.35	0.27	0.59	0.38	0.37	0.38	0.42	0.32
Nb	5.20	5.60	5.20	2.30	6.70	6.60	7.30	8.90	5.10	5.10
Nd	22.50	24.7	21.2	16.0	31.0	25.2	24.5	16.3	14.5	16.6
Ni	32.00	31.0	31.0	19.0	16.0	25.0	42.0	20.0	5.00	15.0
Pb	6.00	6.00	3.00	3.00	8.00	16.0	9.00	8.00	8.00	16.0
Pr	5.33	5.32	4.91	3.06	6.84	6.77	6.04	3.68	2.74	3.35
Rb	3.00	1.00	1.00	12.0	51.0	40.0	25.0	12.0	21.0	9.00

Table 3. (Continued).

Sc	20.6	19.0	20.6	24.4	22.5	15.1	21.7	20.8	23.1	19.2
Sm	4.42	5.24	4.60	3.60	6.12	5.11	5.16	3.17	2.74	3.13
Sn	1.00	1.00	1.00	0.70	1.10	1.20	1.00	0.90	1.20	1.10
Sr	822.1	772.5	781	599.1	527.2	622.9	686.9	826.9	422.3	530.8
Ta	0.59	0.69	0.58	0.40	0.69	0.59	0.73	0.95	0.90	0.75
Tb	0.70	0.76	0.71	0.55	0.93	0.72	0.75	0.54	0.59	0.54
Th	7.80	8.30	7.89	3.39	11.09	15.24	13.39	3.21	1.95	2.92
Tm	0.30	0.37	0.26	0.25	0.43	0.31	0.29	0.33	0.37	0.30
U	1.80	2.70	1.40	0.70	3.20	2.90	2.90	0.70	0.60	0.50
V	231	220	232	239	203	166	208	285	335	294
Y	25.8	27.7	22.2	19.7	33.1	20.9	23.5	16.7	19.7	16.3
Yb	3.10	3.10	2.80	2.60	3.80	2.50	2.80	2.40	2.70	2.30
Zn	95.0	90.0	89.0	125	91.0	78.0	89.0	105	118	115
Zr	111	105	109	53.0	180	129	136	74.	75.0	50.0

$FeOt = FeO + 0.899*Fe_2O_3$

$FeO/Fe_2O_3+FeO = FeO/FeOt=0.88 --(0/0016*SiO_2) - 0.027*(Na_2O+K_2O)$

$(FeOt - FeO)*1.1 = Fe_2O_3$

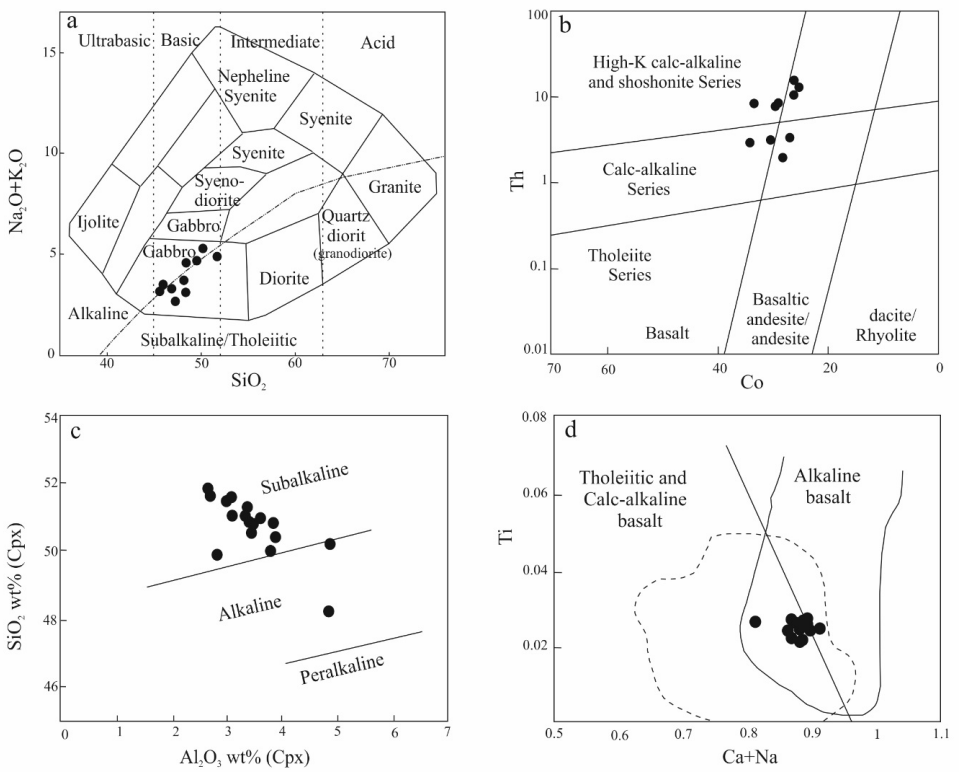

Figure 5. (a) Classification diagram of SiO_2 (wt%) versus $Na_2O + K_2O$ (wt%) (Cox et al., 1979). (b) Co (ppm) versus Th (ppm) diagram for determination magmatic series of the studied gabbros (Hastie et al., 2007). (c) Al_2O_3 versus SiO_2 diagram based of clinopyroxene composition for determination of magmatic series (Le Bas, 1962). (d) Ti versus Na + Ca cations diagram of determining the type of magma based on clinopyroxene composition (Leterrier et al., 1982).

limited and positively correlated with each other; this may indicate the limited magmatic differentiation in the parent magma. Besides, although in petrographic studies, different textural forms of plagioclase were introduced in these rocks, in the results of electron microprobe analysis, no significant difference is seen in the composition of these forms. This may be due to the fact that the parent magma of these rocks did not have extensive magmatic differentiation. The textural characteristics of the studied gabbro show that the crystallization sequence in the parent magma started with the formation of olivine and then olivine + clinopyroxene. The presence of comagmatic enclaves (Figure 4-f), containing altered and anhedral olivines and diopsidic clinopyroxenes, indicates the first crystallizing phases. These minerals are likely to form at the beginning of the crystallization process, settle to the bottom of the magmatic reservoir, and then rise with the magma. With decreasing temperature and pressure at higher levels, clinopyroxene crystals (diopside-salite composition) and plagioclase with labradorite composition formed simultaneously. The orthopyroxene crystals, which have resorption rims and amphibole coronas found in some of these rocks, may have formed at this stage or earlier (Helmy et al., 2008). Furthermore, it could be the result of a late alteration of a magmatic feature. At the end of the crystallization, which probably occurred at the highest levels of the crust and at the final location of emplacement, the crystallization sequence ended with the formation of fine-grained clinopyroxene and plagioclase at the eutectic point and the formation of intergranular texture in the groundmass. Some researchers stated that zoning in clinopyroxenes results from changes in pressure and variable conditions of oxidation and oxygen fugacity (Aydin et al., 2009). Decomposition and corrosion in clinopyroxene can occur due to the reaction of melt and crystal during the crystallization process. In this case, the change in magmatic conditions causes the crystal to change from stable to unstable and decompose (Cox, 1979). The incorporation (infiltration) of aqueous fluids into the magma and increase of oxygen fugacity are also associated with the formation of amphibole corona, resorption and dissolution of clinopyroxene and plagioclase, and forming sieve texture within them. This process may occur after the formation of coarse-grained crystals and before the final emplacement of gabbroic intrusions. Besides, multiple pulses of melt injection into the magma reservoirs and changes in magma composition and temperature, as well as decreasing pressure during magma ascent via the surface (Pearce et al., 1987), are commonly suggested as reasons for the formation of sieve textures. Plagioclase crystals with zoning and sieve textures can result from repeated changes in pressure or volatile content (Nelson and Montana, 1992).

Significant Eu anomalies are not evident in the chondrite-normalized REE diagrams of the studied rocks (Figure 6). The lack of positive anomaly may have been due to an increase in fO_2 in the magma during differentiation (Rollinson, 1993). In this state, as the crystallization progresses, the fO_2 gradually increases, and Europium becomes Eu^{+3}, therefore, its distribution coefficient in plagioclase would have decreased. In less differentiated samples (such as sample N236), the parent magma was more basic (mafic), and the crystallization conditions were still reduced. At this time, Eu^{+2} was

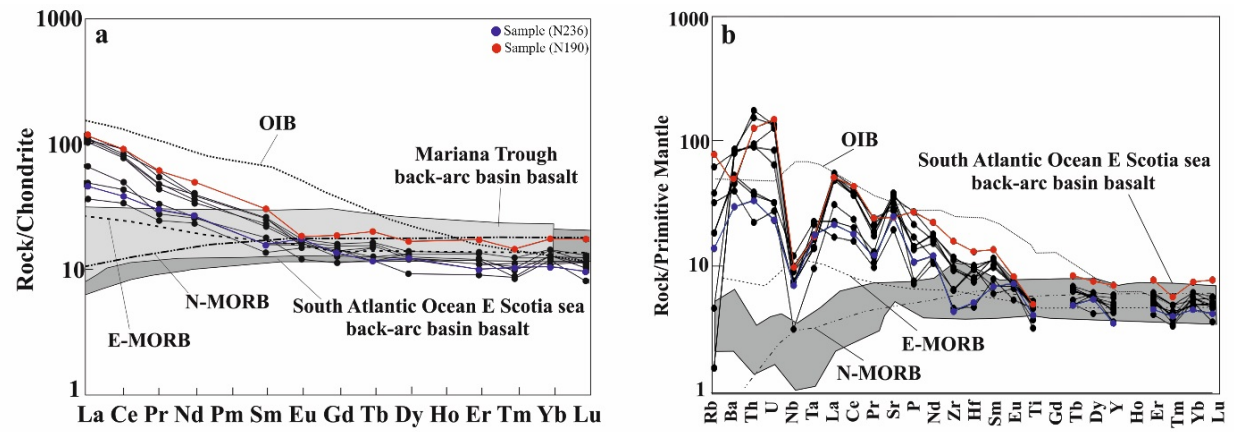

Figure 6. (a) Distribution of rare earth elements of studied gabbro normalized to chondrite (Nakamura, 1974). (b) Spider diagram of trace elements normalized to the primitive mantle (Sun and McDonough, 1989). OIB, N-MORB, and E-MORB values from McDonough and Sun (1995) and data on back-arc basalts in the South Atlantic Ocean East Scotia Sea and Mariana Trough from Liao et al. (2018).

more abundant in the environment and was substituted into the Ca site in plagioclase. In the normalized REE pattern of the same samples, Eu shows a slight positive anomaly. However, in more differentiated samples (such as N190), due to the progress of crystallization or the entry of water or crustal material into the crystallizing magma, fO_2 rises, oxidizing to Eu^{+3}. Thus, it seems that the parent magmas of the studied rocks have gone through history from reduction to oxidation.

One of the characteristic features in the studied rocks is the enrichment of LILE and LREE. In the primitive mantle-normalized diagram (Figure 6-b), the amount of HFSE, which is less mobile in fluid environments, is less than in MORB, whereas the amount of LILE is higher than MORBs. This means that the source rock of the primary magmas has undergone one or more partial melting stages and, as a result, the magma has been depleted in all the elements in Figure 6-b. Indeed, it was even more depleted than source rock of the MORBs. This condition can be seen in the mantle wedge peridotites of the supra-subduction zones (Pearce, 1983), but the enrichment of LILE, U, and Sr and in Figure 6–b shows that after the partial melting and depletion events, a process of enrichment of LILE has occurred and increases the amount of these elements. This enrichment can be due to the digestion of crustal material or the enrichment of source rocks or both, whereas, immobile elements such as Zr, Nb, and Ti have not been able to enter the magma from the rock, and therefore their amount in the magma has decreased and they show depletion in Figure 6-b.

The SiO_2 varies from 45.6 to 51.69 wt. %, and the maximum amount of MgO and Mg# is 5.51 wt. % and 39.31, respectively. More basic samples (such as N113) contain up to 10 vol% olivine, 20% clinopyroxene (diopside-salite), and 35 vol% plagioclase (labradorite). This evidence suggests that their primitive magmas may have been derived from the upper mantle, but they underwent many changes, including magmatic differentiation and enrichment of incompatible elements. Geochemical evidence, such as negative anomalies of Nb, Ta, and Ti and also high Ta/Nb ratio in these rocks (avg: 0.12) (Ta/Nb: 0.06 in the primary mantle) (Wood et al., 1979), are consistent with fluid metasomatism and incompatible elements enrichment in suprasubduction zone environment. Previous works on the magmatic rocks of the Dehaj-Sarduieh volcano-plutonic belt have also emphasized that the lithospheric

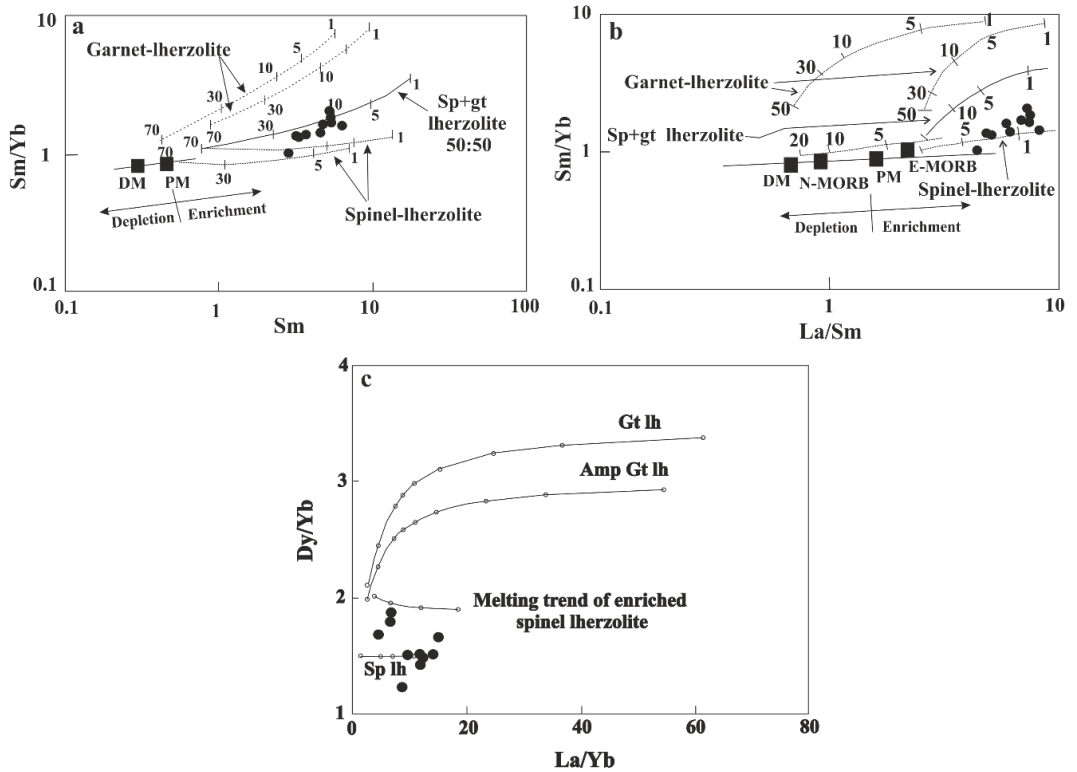

Figure 7. Situation of the studied gabbro samples on the partial melting curves. (a) Sm versus Sm/Yb diagram (b) La/Sm versus Sm/Yb diagram (Aldanmaz et al., 2000). (c) La/Yb versus Dy/Yb diagram (Xie et al., 2015).

mantle in this belt is affected by mantle metasomatism and due to the addition of melts from the descending Neo-Tethys lithosphere, the lithospheric mantle has been enriched in LILE (Dargahi et al., 2010; Behpour et al., 2019). The Nb/U = 4.87 and Nb/Th = 1.1 ratios in the gabbros are close to the primitive mantle. In addition, Th/La = 0.24, Th/U = 4.47, and Zr/Nb = 18.14 ratios in the studied rocks are close to typical mantle ratios (see Rudnick, 2000), which indicates other evidence for the enrichment of the mantle source rock in this region.

The incorporation of crustal material into mantle-derived magmas occurs through various processes. Contamination of magma in crustal reservoirs can change the composition of magmas. The presence of mafic enclaves (Figure 4-f) and the presence of disequilibrated textures in plagioclase and pyroxene in the studied rocks can indicate the contamination process. However, more detailed studies should be used to confirm these events. The studied gabbroic intrusions were emplaced in the continental environment. Thus, their parent magmas can be partially contaminated in crustal reservoirs during ascent. The high ratio of Th/Ta (11.63) and the depletion of Nb and Ta relative to Zr and Hf in the studied rocks reinforce this theory.

Thus, the partial melting of a metasomatized mantle enriched in LILE appears to have formed primary basaltic magmas. Then, the ascent of these magmas into the crust of the Central Iranian microcontinent is accompanied by the processes of fractional crystallization and crustal assimilation (AFC) and has formed the parental magma.

Sm/Yb and La/Sm ratios were used to identify the nature of source peridotites and the possible degrees of partial melting (Figure 7). The studied gabbros are located along the E-MORB side and near the spinel lherzolite melting curve and show that the primary magmas originated from a mantle that was slightly deeper than the spinel lherzolite stability field, forming by about 10%–20% partial melting. Mckenzie and Onions (1991) suggest that one of the reasons for the enrichment of LREE relative to HREE and the flat pattern of HREE in rocks could be that the source rock of the primary magmas is spinel lherzolite.

Plank (2005) showed that low Nb/U ratios (5–20) indicate the metasomatized lithospheric mantle as a source rock, with an average ratio of 4.87 for the studied gabbros, indicating a metasomatized lithospheric source. Also, in magmas whose enrichment has occurred in the subduction environment due to the slab-derived fluids, the amount of Th/Yb showed an increasing trend (Figure

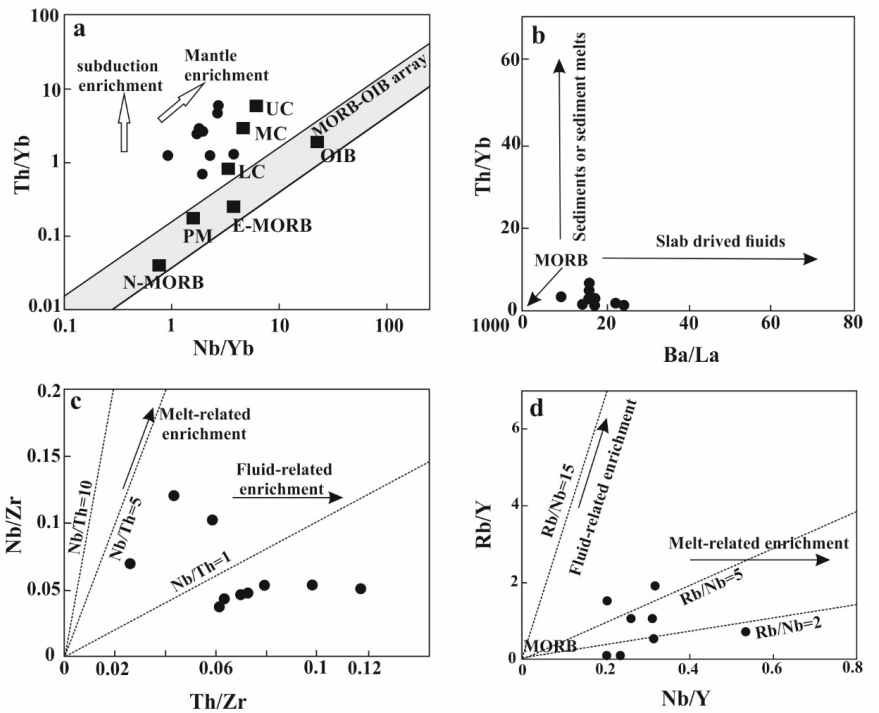

Figure 8.)a) Nb/Yb versus Th/Yb diagram proposed by Pearce (2008), which shows the mantle enrichment for the studied samples. The lower crust (LC), middle crust (MC), and upper crust (UC) data from Rudnick and Gao (2003).)b) Ba/La versus Th/Yb diagram to investigate the effect of fluids or melts on mantle metasomatism (Woodhead et al., 2001). Th/Zr vs. Nb/Zr (c) and Nb/Y vs. Rb/Y (d) diagrams (Zhao and Zhou, 2007) showing the enrichment of the source rocks in the studied area occurred by fluids.

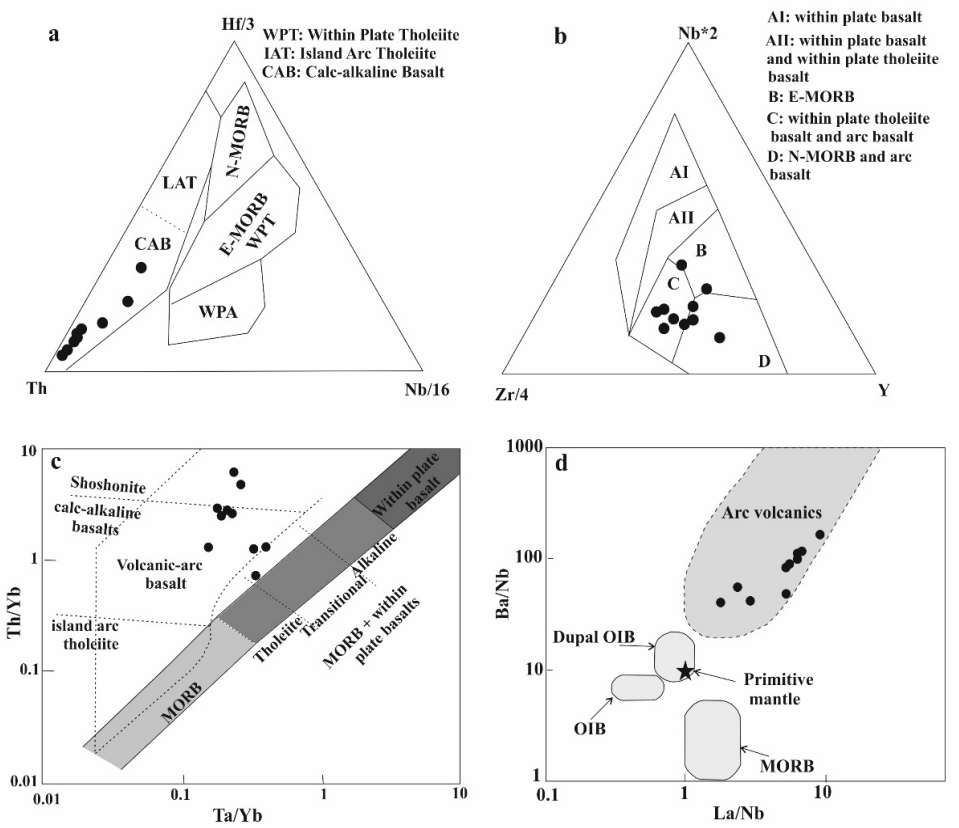

Figure 9. Diagrams determining the tectonic environment showing the studied gabbros plot in the field of arc basalts. (a) Hf/3- Th-Nb/16 diagram from Wood (1980). (b) Nb*2-Zr/4- Y diagram from Meschede (1986). (c) Ta / Yb vs. Th / Yb Diagram (Pearce, 1983). (d) La/Nb vs. Ba/Nb diagram (LaFleche, 1998), MORB, Primitive mantle, OIB, and Dupal OIB data from Sun and McDonough (1989).

8-a). In addition, the high Ba/Nb ratio (85.71) in the gabbros indicates a subduction-related setting, indicative of enrichment of the mantle in this tectonic setting (Plank, 2005). Rb, Ba, K enrichment, as well as high K/Nb and La/Nb, are usually attributed to the lithosphere enriched by slab-derived fluids (Rollinson, 1993), as well as the studied gabbros. In addition, as evident in Figure 8-b, c, d, the primary magma of the studied rocks can be the product of the reaction between the slab-derived fluids and the lithospheric mantle (Zhao and Zhou, 2007).

5.2. Tectonic setting

Various studies have shown that tectonomagmatic evolution of the Urmia-Dokhtar magmatic belt is closely related to the subduction of the Neo-Tethys lithosphere beneath central Iran (Berberian and King, 1981; Alavi, 1994). This study situated south of Bardsir (in Kerman province) is consistent with those findings. The most important magmatic phase in the Dehaj-Sarduieh belt is related to the Eocene period, during which a large volume of basaltic to intermediate lava flows and their associated pyroclastic rocks formed and very thick volcano-sedimentary assemblages in this belt were produced (Dimitrijevic, 1973; Shafiei et.al., 2008). The formation of this huge volume of magma has been attributed to the melting of a mantle wedge above the Neo-Tethys subduction zone and ascent, resulting in the emplacement of magmas into the continental margin (Central Iran) (Berberian and King, 1981; Alavi, 1994; Mohajjel et al., 2003) or to intercontinental rifting (Sabzehei, 1974; Amidi and Michel, 1985).

Detailed field studies show that these gabbros situated south of Bardsir after the formation of Eocene-aged lava flows and pyroclastic rocks, clearly intruded into them through fractures and hence have been formed after the Eocene period. As shown in the Hf-Th-Nb and Nb-Zr-Y ternary diagrams (Figure 9-a, b), these gabbros fall in the field of calc-alkaline basalts and arc-related environment. Also in Figures 9-c and 9-d, the gabbros plot in the arc basalt field. To determine whether the arc was continental

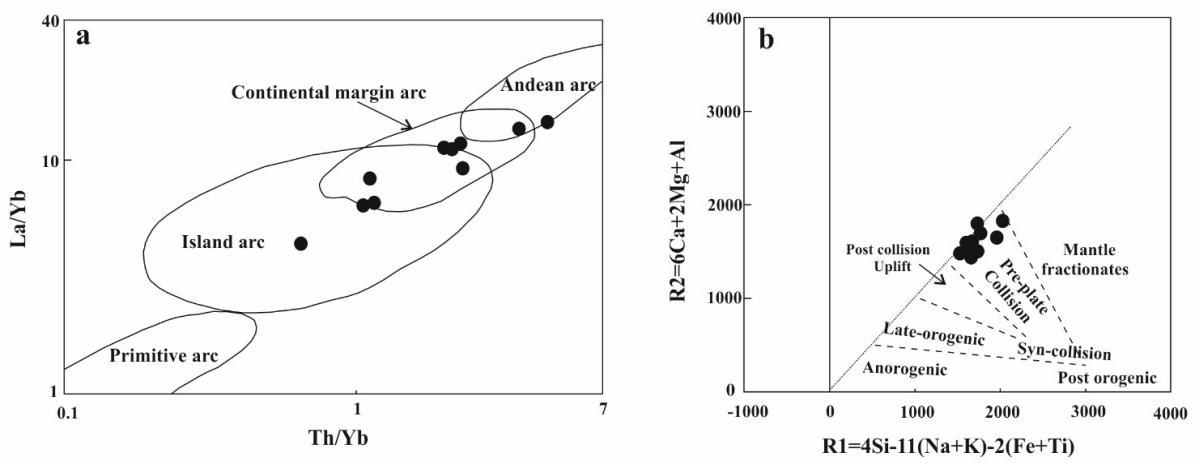

Figure 10. (a) Th/Yb vs. La/Yb diagram (Condie, 1989) shows the studied rocks fall in the field of continental margin arc. (b) Graph R1 vs. R2 (Batchelor and Bowden, 1985) shows the pr-collision situation for the gabbros.

or oceanic, the La/Yb versus Th/Yb diagram was used (Figure 10-a), falling into the continental arc field. Various authors suggest different times for the collision between the Arabian plate and central Iran. Alavi (1994) suggests Late Cretaceous, Allen and Armstrong (2008) Late Eocene, McQuarrie et al. (2003) Early Miocene to Middle Miocene, Shahabpour (2007) Late Miocene, and Dargahi et al. (2010) suggested Late Eocene for this process. On the other hand, all researchers concur that the post-Miocene magmatic activities in Urmia Dokhtar are postcollision magmatic episodes. To investigate the emplacement period of these gabbro intrusions relative to the collision timing, a schematic diagram presented in Figure 10-b was used, showing that the samples belong to an episode of precollision magmatism. Thus, it seems that the parent magmas of the gabbros in the south of Bardsir have been formed in a continental arc environment and penetrated the Eocene magmatic complex before the collisional event (Figure 11).

Studies conducted on magmatic intrusions in other parts of UDMA have also clarified the nature of magmatism related to the upper mantle and lower crust in this part of Iran.

Kazemi et al., (2019) attributed 40 ma aged Boin Zahra granitoids (central part of UDMA), to precollision environment. The gabbros of southern Bardsir, clearly penetrated into the Oligocene granitoids (Sepidbar, 2019) and therefore, they also must belong to the precollision environment. In addition, Babazadeh et al., (2017; 2019) by working on Oligocene-Miocene granitic to gabbroic intrusions in the central parts of DUMA, revealed that the emplacement of these intrusions was related to the subduction of the Neo-Tethys beneath Central Iran and formation of gabbro intrusions similar to those in Southern Bardsir continued until the late Miocene. So, this evidence confirms the precollision environment for the studied intrusions.

Similar masses were also studied by Fazlnia (2019) in the northwest of UDMA and attributed to the syn- or postcollision. While (Kananian et al., 2014) showed that the older massifs of the Dom mountain (Oligocene) in the central parts of UDMA belong to the continental margin arc environment. Zheira et al. (2020) presented geochemical, isotopic, and geochronological evidence from gabbroic and volcanic rocks at the central parts of UDMA and indicate three major phases of magmatic activity in that region during late Eocene to Miocene, resulting in complex tectonic regime transition from compressional subduction to extensional postcollisional settings. Recently Mokhtari et al. (2022) by geochemistry and age dating data on the UDMA igneous rocks, presented high flux magmatic events betwen 53– 37 Ma and attributed these events to precollision magmatism.

According to field studies, faults and fractures in the region are important factors in controlling the trends of dykes. These controlling structures are key to the overall geodynamic setting and timing of emplacement. Typically, uplift is associated with magmatic underplating that causes late extension throughout the late arc evolution with the arc modified enough to limit assimilation and allow for more rapid ascent (with less contamination). Also, these types of hypabyssal dykes and stocks can feed extrusive.

Conclusions

Petrogenetic studies of gabbroic intrusions in the southeastern part of the Urmia-Dokhtar magmatic belt

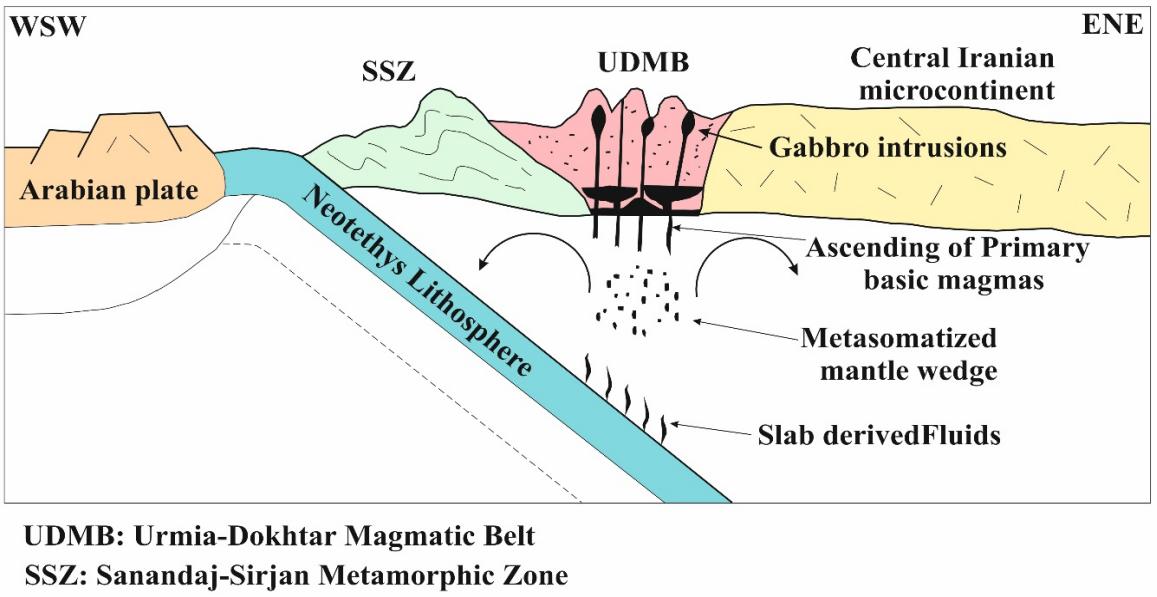

Figure 11. Schematic illustration showing ascending and intrusion style of the Bardsir gabbroic intrusions and their situation relative to the main structural units in southeastern Iran (see the text for details).

helped clarify the nature of the lithospheric mantle beneath this region. Field, petrographic, and geochemical evidence showed that the source of these intrusions was spinel lherzolite, which first endured the partial melting process and then suprasubduction zone metasomatism resulting from subducting oceanic slab-derived fluids. The resulting melt underwent fractional crystallization and assimilation during the ascent and cooling in the various lithospheric magmatic reservoirs. They were then emplaced in a continental margin environment. The intrusion occurred after the Eocene and before the collision of the Arabian plate with the central Iranian microcontinent. Major fractures in the region controlled the intrusion of the gabbro bodies.

Acknowledgments

This research forms part of the PhD study of the first author financially supported by the Shahid Bahonar University of Kerman. We acknowledge Prof. David Lentz for their constructive comments leading to important improvements in the manuscript. The authors sincerely wish to thank the journal manager and reviewers who critically reviewed the manuscript and made valuable suggestions.

References

Afsharianzadeh M, Etemadi N (1992). Geological map of Bardsir, Kerman province. Geological Survey of Iran.

Alavi M (1994). Tectonics of the Zagros orogenic belt of Iran: new data and interpretations. Tectonophysics 229 (3): 211-238. https://doi.org/10.1016/0040-1951(94)90030-2

Allen M-B, Armstrong H-A (2008). Arabia–Eurasia collision and the forcing of mid-Cenozoic global cooling. Palaeogeography, Palaeoclimatology, Palaeoecology 265 (1): 52-58. https://doi.org/10.1016/j.palaeo.2008.04.021

Aldanmaz E, Pearce J-A, Thirlwall M, Mitchell J (2000). Petrogenetic evolution of late Cenozoic, post-collision volcanism in western Anatolia, Turkey. Journal of Volcanology and Geothermal Research 102 (1-2): 67-95.

Amidi S-M, Michel R (1985). Cenozoic magmatism of the Surk area (central Iran) stratigraphy, petrography, geochemistry and their geodynamic implications. Alpine Geology 61: 1-16.

Aydin F, Karsli O, Sadiklar MB (2009). Compositional variations, zoning types and petrogenetic implications of low-pressure clinopyroxenes in the Neogene alkaline volcanic rocks of northeastern Turkey. Turkish Journal of Earth Sciences 18 (2): 163-186.

Babazadeh S, D'Antonio M, Cottle J-M, Ghalamghash J, Raeisi D et al. (2021). Constraints from geochemistry, zircon U-Pb geochronology and Hf-Nd isotopic compositions on the origin of Cenozoic volcanic rocks from central Urumieh-Dokhtar magmatic arc, Iran. Gondwana Research 90: 27-46.

Babazadeh S, Ghorbani M-R, Bröcker M, D'Antonio M, Cottle J et al. (2017). Late Oligocene–Miocene mantle upwelling and interaction inferred from mantle signatures in gabbroic to granitic rocks from the Urumieh–Dokhtar arc, south Ardestan, Iran. International Geology Review 59 (12): 1590-1608.

Babazadeh S, Ghorbani M-R, Cottle J-M, Bröcker M (2019). Multistage tectono-magmatic evolution of the central Urumieh–Dokhtar magmatic arc, south Ardestan, Iran: Insights from zircon geochronology and geochemistry. Geological Journal 54 (4): 2447-2471.

Basta M-S (2015). Petrology and geochemical characteristic of the Younger Gabbros of Wadi Shianite area, southeastern Desert, Egypt. Open Journal of Geology 5 (8). https://doi.org/10.4236/ojg.2015.58052

Batchelor R-A, Bowden P (1985). Petrogenetic interpretation of granitoid rock series using multicationic parameters. Chemical Geology 48 (1-4): 43-55.

Behpour S, Moradian A, Ahmadipour H, Nakashima K (2019). Mineralogy, petrology and geochemistry of mafic dikes in the southeast Jebal-E-Barez Granitoids (Bam, Kerman province, Iran): Studies from mafic dikes formed in a volcanic arc-setting. Turkish Journal of Earth Sciences 28: 920-938.

Berberian M, King G (1981). Towards a paleogeography and tectonic evolution of Iran. Canadian Journal of Earth Sciences 18 (2): 210-265.

Condie K-C (1989). Geochemical changes in basalts and andesites across the Archean-Proterozoic boundary: Identification and significance. Lithos 23 (1): 1-18. https://doi.org/10.1016/0024-4937(89)90020-0

Cox K-G, Bell J-D, Pankhurst R-J (1979). The Interpretation of the Igneous Rocks. London: George Allen & Unwin. 450 p.

Daieparizi M, Ahmadipour H, Moradian A (2021). Introduction and characterization of Neogene volcanic eruptions in Pariz area (Kerman province) and their petrological features using pyroclastic deposits. Scientific Quarterly, Geosciences 31: 25-36.

Dargahi S, Arvin M, Pan Y, Babaei A (2010). Petrogenesis of post-collisional A-type granitoids from the Urumieh–Dokhtar magmatic assemblage, southwestern Kerman, Iran: constraints on the Arabian–Eurasian continental collision. Lithos 115 (1-4): 190-204.

Deng Y-F, Song X-Y, Chen L-M, Zhou T, Pirajno F et al. (2014). Geochemistry of the Huangshandong Ni–Cu deposit in northwestern China: implications for the formation of magmatic sulfide mineralization in orogenic belts. Ore Geology Reviews 56: 181-198.

Dimitrijevic MD (1973). Geology of Kerman region. Geological Survey of Iran, Report no. 52, 334 p.

Fazli N, Ghaderi M, Movahednia M, Li J-W, Lentz D-R et al. (2022). Geology and genesis of the North Narbaghi Cu-Ag deposit in the Urumieh-Dokhtar magmatic arc, Iran: Fluid inclusion and stable isotope constraints. Ore Geology Reviews 144: 104801. https://doi.org/10.1016/j.oregeorev.2022.104801

Fazlnia A (2019). Geochemical and tectonic significance of the Arbat alkali gabbro-monzonite-syenite intrusions, Urumieh–Dokhtar Magmatic Arc, Iran. Geological Quarterly 63 (1): 16-29.

Hastie A-R, Kerr A-C, Pearce J-A, Mitchell S-F (2007). Classification of altered volcanic island arc rocks using immobile trace elements: development of the Th-Co discrimination diagram. Journal of Petrology 48: 2341-2357.

Helmy H-M, Yoshikawa M, Shibata T, Arai S, Tamura A (2008). Corona structure from arc mafic-ultramafic cumulates: the role and chemical characteristics of late-magmatic hydrous liquids. Journal of Mineralogical and Petrological Sciences 103 (5): 333-344.

Kananian A, Sarjoughian F, Nadimi A, Ahmadian J, Ling W (2014). Geochemical characteristics of the Kuh-e Dom intrusion, Urumieh–Dokhtar Magmatic Arc (Iran): Implications for source regions and magmatic evolution. Journal of Asian Earth Sciences 90: 137-148.

Kazemi K, Kananian A, Xiao Y, Sarjoughian F (2019). Petrogenesis of Middle-Eocene granitoids and their Mafic microgranular enclaves in central Urmia-Dokhtar Magmatic Arc (Iran): Evidence for interaction between felsic and mafic magmas. Geoscience Frontiers 10 (2): 705-723.

LaFleche M-R, Camire G, Jenner G-A (1998). Geochemistry of post-Acadian, Carboniferous continental intraplate basalts from the Maritimes Basin, Magdalen Islands, Quebec, Canada. Chemical Geology 148: 115–136.

Le Base M-J (1962). The role of aluminum in igneous clinopyroxenes with relation to their parentage. American Journal of Science 260: 267–288.

Leterrier J, Maury R-C, Thonon P, Girard D, Marchal M (1982). Clinopyroxene composition as a method of identification of the magmatic affinities of Paleo-volcanic series. Earth and Planetary Science Letters 59: 139–154.

Liao F, Wang Q, Chen N, Santosh M, Xu Y et al. (2018). Geochemistry and geochronology of the~ 0.82 Ga high–Mg gabbroic dykes from the Quanji Massif, southeast Tarim Block, NW China: implications for the Rodinia supercontinent assembly. Journal of Asian Earth Sciences 157: 3-21.

McBirney A-R (2009). Factors governing the textural development of Skaergaard gabbros: A review. Lithos 111 (1): 1-5. https://doi.org/10.1016/j

McDonough W-F, Sun S-S (1995). The composition of the Earth, Chemical Geology 120: 223–253.

McKenzie D, O'Nions R (1991). Partial melt distributions from inversion of rare earth element concentrations. Journal of Petrology 32 (5): 1021-1091.

McQuarrie N, Stock J, Verdel C, Wernicke B (2003). Cenozoic evolution of Neotethys and implications for the causes of plate motions. Geophysical Research Letters 30 (20).

Meschede M (1986). A method of discriminating between different types of mid-ocean ridge basalts and continental tholeiites with the Nb-Zr-Y diagram. Chemical Geology 56 (3): 207-218. https://doi.org/10.1016/0009-2541(86)90004-5

Mohajjel M, Fergusson C, Sahandi M (2003). Cretaceous–Tertiary convergence and continental collision, Sanandaj–Sirjan zone, western Iran. Journal of Asian Earth Sciences 21 (4): 397-412.

Mokhtari M-A-A, Kouhestani H, Pang K-N, Hsu S-C, Chung S-L et al. (2022). Early Eocene high-Sr/Y magmas from the Urumieh-Dokhtar paleo-arc, Iran: Implications for the origin of high-flux events in magmatic arcs. Lithos 416-417: 106656. https://doi.org/10.1016/j.lithos.2022.106656

Nakamura N (1974). Determination of REE, Ba, Mg, Na and K in carbonaceous and ordinary chondrites. Geochimica et Cosmochimica Acta 38: 757-775.

Nelson ST, Montana A (1992). Sieve-textured plagioclase in volcanic rocks produced by rapid decompression. American Mineralogist 77 (11-12): 1242-1249.

Pearce J-A (1983). Role of the sub-continental lithosphere in magma genesis at active continental margins. In: Hawkesworth CJ, Norry MJ eds. Continental basalts and mantle xenoliths, Nantwich, Cheshire: Shiva Publications 230-249.

Pearce J-A (2008). Geochemical fingerprinting of oceanic basalts with applications to ophiolite classification and the search for Archean oceanic crust. Lithos 100 (1): 14-48. https://doi.org/10.1016/j.lithos.2007.06.016

Pearce T, Russell J, Wolfson I (1987). Laser-interference and Nomarski interference imaging of zoning profiles in plagioclase phenocrysts from the May 18, 1980, eruption of Mount St. Helens, Washington. American Mineralogist 72 (11-12): 1131-1143.

Plank T (2005). Constraints from thorium/lanthanum on sediment recycling at subduction zones and the evolution of the continents. Journal of Petrology 46 (5): 921-944.

Raeisi D, Zhao M, Babazadeh S, Long L-E, Hajsadeghi S et al. (2021). Synthesis on productive, sub-productive and barren intrusions in the Urumieh-Dokhtar magmatic arc, Iran, constraints on geochronology and geochemistry. Ore Geology Reviews 132: 103997.

Rollinson H-R (1993). Using Geochemical Data: evaluation, presentation, interpretation. London: Longman Scientific and Technical.

Ross P-S, Bédard J-H (2009). Magmatic affinity of modern and ancient sub-alkaline volcanic rocks determined from trace-element discriminant diagrams. Canadian Journal of Earth Sciences 46 (11): 823-839.

Rudnick R-L, Barth M-G, McDonough W-F, Horn I (2000). Rutile-bearing refractory eclogites: missing link between continents and depleted mantle. Journal of Science 287 (5451): 278-281.

Rudnick R-L, Gao S (2003). The Composition of the Upper Crust. Pp 1-64 in HD Holland & KK Turekian (eds.): Treatise on Geochemistry 3: Elsevier.

Sabzehei M (1974). The ophiolitic mixtures of the Esfandagheh region (Southern Iran): petrological and structural study, interpretation in the Iranian setting. Unpublished Thesis. Scientific and Medical University of Grenoble, France.

Salehi Nejad H, Ahmadipour H, Moinzadeh H, Moradian A, Santos J-F (2021). Geochemistry and petrogenesis of Raviz-Shanabad intrusions (SE UDMB): an evidence for Late Eocene magmatism. International Geology Review 63 (6): 717-734.

Sepidbar F, Ao S, Palin R-M, Li Q-L, Zhang Z (2019). Origin, age and petrogenesis of barren (low-grade) granitoids from the Bezenjan-Bardsir magmatic complex, southeast of the Urumieh-Dokhtar magmatic belt, Iran. Ore Geology Reviews 104: 132-147.

Shafiei B, Shahabpour J, Haschke M (2008). Transition from Paleogene normal calc-alkaline to Neogene adakitic-like plutonism and Cu-Metallogeny. In The Kerman Porphyry Copper Belt: Response to Neogene Crustal Thickening. Journal of Sciences Islamic Republic of Iran 19 (1).

Shahabpour J (2007). Island-arc affinity of the Central Iranian Volcanic Belt. Journal of Asian Earth Sciences 30 (5): 652-665. https://doi.org/10.1016/j.jseaes.2007.02.004

Sun S-S, McDonough W-F (1989). Chemical and isotopic systematics of oceanic basalts: implications for mantle composition and processes. In: Saunders AD, Norry MJ (Eds.), Magmatism in the Ocean Basins. Geological Society of London 42: 313–345.

Whitney D-L, Evans B-W (2010). Abbreviations for names of rock-forming minerals. American Mineralogist 95 (1): 185-187.

Wood D-A (1980). The application of a Th-Hf-Ta diagram to problems of tectonomagmatic classification and to establishing the nature of crustal contamination of basaltic lavas of the British Tertiary Volcanic Province. Earth and Planetary Science Letters 50 (1): 11-30.

Woodhead JD, Hergt JM, Davidson JP, Eggins SM (2001). Hafnium isotope evidence for 'conservative' element mobility during subduction zone processes. Earth and Planetary Science Letters 192 (3): 331-346. https://doi.org/10.1016/S0012-821X(01)00453-8

Xie Q, Zhang Z, Hou T, Santosh M, Jin Z et al. (2015). Petrogenesis of the Zhangmatun gabbro in the Ji'nan complex, North China Craton: Implications for skarn-type iron mineralization. Journal of Asian Earth Sciences 113: 1197-1217.

Yang Q-Y, Santosh M, Dong G (2014). Late Palaeoproterozoic post-collisional magmatism in the North China Craton: geochemistry, zircon U–Pb geochronology, and Hf isotope of the pyroxenite–gabbro–diorite suite from Xinghe, Inner Mongolia. International Geology Review 56 (8): 959-984. https://doi.org/10.1080/00206814.2014.908421

Zhao J-H, Zhou M-F (2007). Geochemistry of Neoproterozoic mafic intrusions in the Panzhihua district (Sichuan Province, SW China): Implications for subduction-related metasomatism in the upper mantle. Precambrian Research 152 (1): 27-47. https://doi.org/10.1016/j.precamres.2006.09.002

Zheira G, Masoudi F, Rahimzadeh B (2020). Geochemical constraints on Eocene–Miocene geodynamic and magmatic evolution of the Varan-Naragh area, Urumieh-Dokhtar Magmatic Arc, Iran. Canadian Journal of Earth Sciences 57 (9): 1048-106.